Journal of Electroceramics 1:3, 273–286, 1997

Energy-Related Applications of Nanostructured Carbons

M.S. DRESSELHAUS & G. DRESSELHAUS
Massachusetts Institute of Technology, Cambridge, MA 02139

Abstract. A wide range of nanostructured π-bonded carbon-based materials, with unique physical properties is presented, including carbon fibers, carbon nanoparticles, porous carbons, fullerenes and carbon nanotubes. Particular emphasis is given to future research directions in these nanostructured carbon-based materials and to energy-related applications that may result.

Keywords: carbons, nanotubes, fullerenes, nanofibers, aerogels, activated-carbons

1. Unique Physical Properties of Carbons

Carbon materials with π-bonding have for many years been of great interest because of their extreme properties, including the highest strength and stiffness to weight ratio, among the highest reported thermal conductivity, and anisotropy in transport and optical properties. In the past decade a number of fascinating, new nanostructured π-bonded carbon phases have been discovered and studied, and because of their unique properties, specific energy-related applications are expected. These properties and applications are reviewed in this chapter.

Of the various novel π-bonded carbon-based materials that have been discovered recently C_{60} has been the most noteworthy because of its uniqueness as an ideal, high symmetry mono-disperse nanoparticle with special properties in the context of nanostructures. The discovery of C_{60} and other fullerenes in 1985 was soon followed by the discovery of carbon nanotubes in 1991. Other carbon nanostructured materials of current interest for energy-related applications include carbon fibers, carbon nanoparticles, and porous carbons, such as activated carbons and carbon aerogels. Carbon materials have for many years been used widely for energy-related applications, such as for electrodes in the manufacture of steel and also as moderators for nuclear reactors, but these materials do not relate to nanostructures, and therefore are not discussed in this chapter.

Because of the vast differences in the structure and properties of the various nanostructured carbon-based materials, as well as the maturity of the R&D in these materials, the various materials categories are presented separately. Some carbon materials such as carbon fibers and porous carbons have already been in part commercialized, while others such as fullerenes and carbon nanotubes are still close to their discovery stage. Thus it is appropriate that the R&D programs for the various carbon-based materials should change with time to meet specific DOE energy needs in the future.

2. Carbon Fibers

Carbon fibers represent an important class of π-bonded carbon materials that have their fiber axes close to an in-plane direction of a graphene layer (loosely called an *a*-axis), whereby a graphene layer is defined as a single layer of crystalline graphite. Although commercial carbon fibers generally have diameters exceeding 1 μm and do not come under the classification of nanostructured carbons, vapor grown carbon fibers are prepared with diameters in the 100 nm range and below. We will restrict our discussion here to this subset of carbon nanofibers. Since the fiber axis for nanofibers is along the *a*-axis, there nanostructures have excellent mechanical properties and high thermal conductivities [1–6].

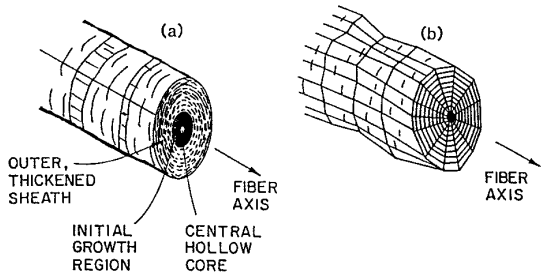

Fig. 1. Sketch illustrating the morphology of vapor grown carbon fibers (VGCF): (a) as-deposited at 1100°C, (b) after heat treatment to 3000°C [1].

Many of the techniques for the vapor growth of carbon nanofibers have also been used recently to synthesize carbon nanotubes.

Vapor grown carbon fibers (see Fig. 1) can be prepared over a wide range of diameters (from less than 1000 Å to more than 100 μm). These fibers, however, are not continuous, but have lengths up to ~30–100 cm, and they have hollow cores. Thus, their morphology bears a significant resemblance to the carbon nanotubes discussed in section 6. The preparation of vapor grown fibers is based on the growth of a thin hollow tube from a transition metal catalytic particle containing super-saturated carbon in solution at 1050°C. The catalytic particles are introduced into the growth chamber in a variety of ways [1], resulting in vapor grown nanofibers with different textures depending on the composition and size of the catalytic particle and the growth temperature. At the innermost part of the thin hollow tube is a carbon nanotube, as shown in Fig. 2 [5]. In the normal growth of vapor grown carbon fibers, the thin hollow tube is thickened through an epitaxial growth process to yield a tubular structure with an onion-skin or tree-ring morphology [see Fig. 1(a)]. Subsequent heat treatment to ~2500°C results in carbon fibers with a tree-ring concentric-cylinder morphology [2], and heat treatment above 3000°C yields faceting of the vapor grown fibers [as shown in Fig. 1(b)]. Carbon nanofibers are available commercially but are sold in small quantities relative to carbon fibers with diameters exceeding 1 μm.

Research on vapor grown carbon fibers has been heightened in recent years by the discovery of carbon nanotubes, because of the close connection between the nanotubes and the vapor grown carbon fibers [7]. Of particular current interest are carbon nanofibers in the diameter range $15 \leq d \leq 100$ nm. This diameter range is especially interesting because in the lower limit these nanofibers are expected to have circular cross sections like carbon nanotubes, while at the upper limit, faceting of the cross section [see Fig. 1(b)] occurs under heat treatment at high temperatures. To date there has been almost no systematic study of carbon nanofibers in the diameter range $15 < d < 100$ nm.

These very thin carbon nanofibers are already finding their way into commercial applications such as electrochemical capacitors [8], conductive additives to plastics [9], and other niche applications, such as a conducting filler of plastics for electromagnetic shielding applications, or as a spray paint using the electrostatic attraction of the paint to an auto part to minimize waste and pollution. The percolation

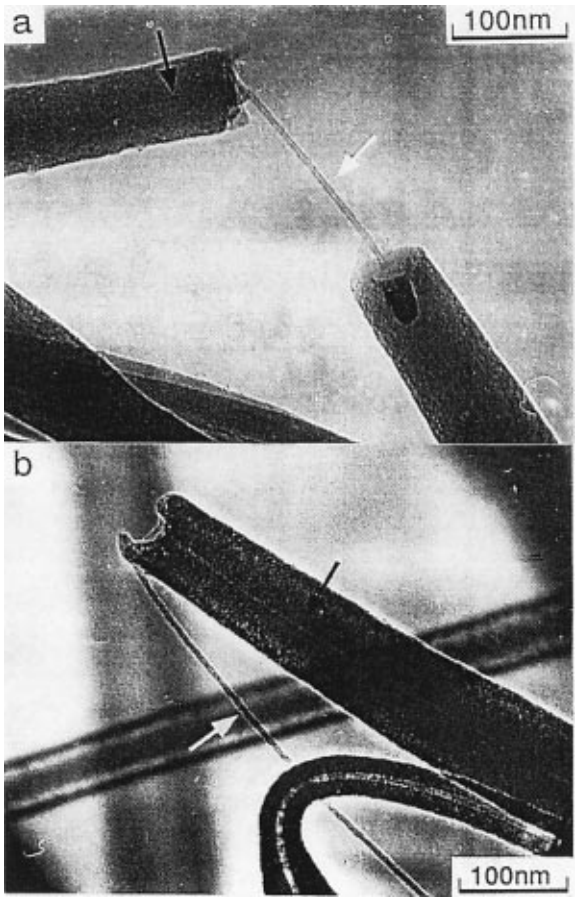

Fig. 2. TEM picture of the broken portion of an as-grown nanofiber cross section exposing the nanotube core at the center of the nanofiber [4].

threshold for nanofibers is very low, so that a very small amount of nanofiber additive is required relative to carbon blacks which are spherical particles, that have in the past been used for conducting filler applications. It would make sense for the DOE to have a small basic research effort on the structure and properties of multi-wall carbon nanotubes [10,11] and on the connection between carbon nanofibers and multi-wall carbon nanotubes. There is also merit in supporting an applied program directed toward energy-related applications not being pursued by the commercial sector, especially giving attention to the synthesis of carbon nanofibers, and to providing the research community with suitable samples for carrying out state-of-the-art research work on nanofibers and multi-wall carbon nanotubes.

3. Carbon Nanoparticles

Carbon nanoparticles may either be of solid carbon or they can be carbon-coated nanocapsules, consisting of carbon layers, wrapped around other materials, usually carbides of transition metals or rare earth materials. A model for the formation of a carbon-coated nanoparticle or nanocapsule (30–70 nm diameter) [12] is shown in Fig. 3.

The filled nanocapsules, such as the one shown schematically in Fig. 3, are synthesized by arc discharge or laser vaporization methods when the carbon electrode or carbon target is fabricated from a mixture of carbon and an appropriate transition metal, rare earth metal, or other species [13]. The carbon coating may consist of a few nanometers of disordered carbon or of polygonized graphene shells, and the carbon layers serve to passivate the core material which is often reactive. Likewise, the core of the nanoparticle is either fully filled or partially filled with a crystalline or disordered carbide phase of the transition metal or rare earth metal, that was previously introduced into the carbon electrode or carbon target. The shape of the carbon structure that is formed depends critically on the growth conditions. These carbon nanocapsules have recently become an active research area in terms of the development of improved synthesis routes, as well as in the study of their structural, magnetic and superconductive properties. The higher melting point rare earth metals or metal carbides tend to form partially filled nanocapsules (see Fig. 3), while transition metal carbides with lower melting points, such as cementite Fe_3C, are more likely to form completely filled capsules [13].

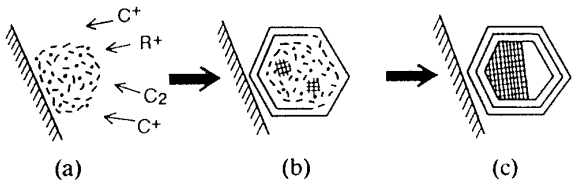

Fig. 3. Schematic model for the growth of a nanocapsule partially filled with a crystallite of rare-earth (R) metal carbide (RC_2 for R = Y, La, ..., Lu; R_3C_4 for R = Sc) using an arc method for synthesis: (a) R-C alloy particles, which may be in a liquid or quasi-liquid phase, are formed on the surface of the cathode; (b) solidification (graphitization) begins from the surface of the nanoparticle, and R-enriched liquid is left inside; (c) the graphite cage (outside) equilibrates with the metal carbide (inside) [13].

In the case of the rare earths, carbon coated YC_2 nanoparticles tend to show faceted graphitic faces with an average turbostratic interlayer distance of 0.344 nm, containing crystalline YC_2 with lattice spacings corresponding to the (002) plane of YC_2, and a void volume or cavity, in addition to the single-crystal YC_2 material. This is consistent with an initial crystallization of the graphitic shell, while the Y-C alloy within the nanoparticle remains molten, as shown in Fig. 3(b). The graphitic shell crystallizes until the YC_2 composition of the melt is reached, when finally there is a crystallization of the YC_2, as shown in Fig. 3(c) [12].

Although most of the current research on carbon nanoparticles is directed toward synthesis, structure, properties and the relation between the nanoparticles and carbon nanotubes, attention is concurrently being given to the development of practical applications of the filled nanoparticles. Magnetic nanoparticles are of particular commercial interest because they can be used for a variety of applications, such as magnetic inks for high speed printing on metal cans. Magnetic carbon nanoparticles are also being mixed with organic dyes to provide components for color xerography applications. In biotechnology there are opportunities to use magnetic particles for applications, such as for contrast agents used in MRI (magnetic resonance imaging), and the attachment of biomolecules such as drugs for a drug delivery system to the outer carbon surface of a nanoparticle. Once the biomolecule has completed its work, the nanoparticle can be retrieved by a magnetic field. Large established companies and small start-up

companies are both involved with these carbon nanoparticle applications, and there has been a strong interaction between researchers in academia and in companies, who are working on these applications. However, companies are not giving much attention to basic research and generic applied research, but are rather directed toward proprietary development work. The DOE therefore has a special role to play in the support of basic science, and of energy-related applications of carbon nanoparticles, especially in areas where companies are not yet working.

Hollow concentric carbon spheres are also formed upon intense electron beam irradiation of carbon nanoparticles with faceted and irregular shapes [14–16] (see Fig. 4). Some of these concentric carbon nano-particles have been found to have an innermost sphere with a diameter of 7.1 Å, which is the same as the diameter of the C_{60} molecule. Spherical shells with diameters up to 100 Å have been synthesized (see Fig. 4), similar to the dimensions reported for small-sized carbon blacks. Although containing a large amount of strain energy, the spherical carbon shells contain no dangling bonds and are stable under further electron bombardment, even when the nanoparticle contains only a few (2–4) spherical shells [17,18].

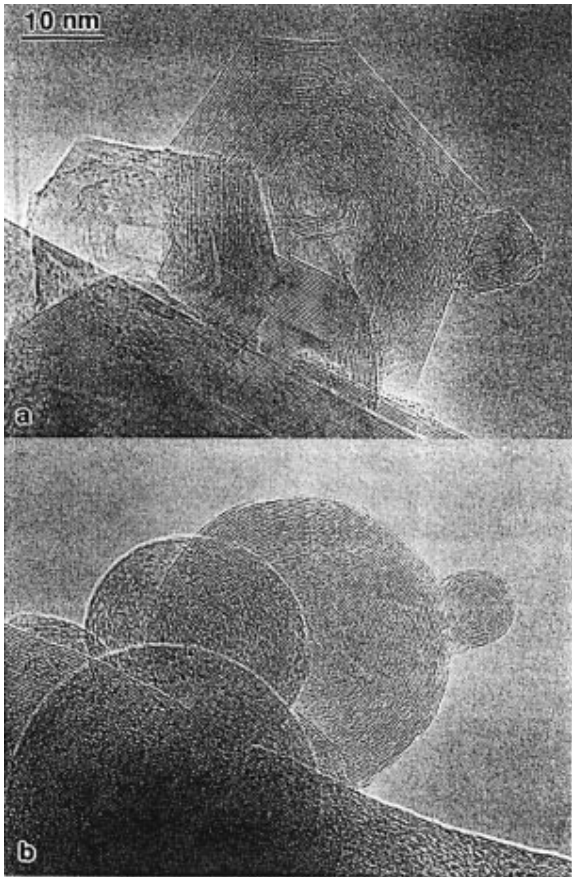

Fig. 4. High-resolution electron micrographs of graphitic nano-particles. (a) As obtained from an electric arc deposit, the nano-particles display a well-defined faceted structure and a large inner hollow space, and (b) the same nano-particles as in (a) after being subjected to intense electron irradiation. The nano-particles now show a spherical shape and a much smaller central empty space [16].

The growth of carbon ''onion'' layers is believed to begin at the surface of the onion-like structure and then to progress toward the center [15,19]. The onion-like carbon nano-particles are stabilized by the energy gain from the weak van der Waals interaction between adjacent carbon shells [18,20,21]. The synthesis and purification of macroscopic quantities of quasi-spherical onion-like nano-particles with a small size distribution remain a major challenge to a systematic study of the properties of carbon onions.

Onion-like multilayer carbon shells can also be generated by shock wave treatment of carbon soot [22], from carbon deposits exposed to a plasma torch [23], by laser melting of carbon within a high-pressure (50–300 kbar) cell [24], and by annealing nano-diamonds at temperatures in the range 1100 to 1500°C [25]. Under certain circumstances, small diamonds have been formed at the center of these carbon shells [27], and this topic is being pursued actively for both scientific and practical reasons. The stress induced by the large curvature of small diameter carbon shells is believed to be responsible for the nucleation of these small diamonds.

Basic studies of carbon onion nano-particles has been pursued only by a few groups, and mostly in Europe. Some greater visibility of US researchers in this subfield might be desirable.

4. Porous Carbons, Activated Carbons and Aerogels

Among the exceptional properties of sp^2 bonded carbons is their ability to form porous materials with very high surface area (up to 3000 m^2/g), low mass densities (below 0.1 g/cm^3), and a high concentration of pores of nanometer dimensions. Examples of porous carbons are activated carbon fibers which

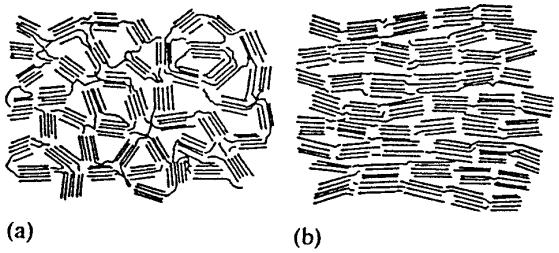

Fig. 5. Schematic model for the microstructure of porous materials. The nanopores for a high surface area activated carbon fiber are shown in (a) where the basic structural units of the micro-graphitic clusters are randomly arranged. The structure of (a) after some heat treatment is shown in (b), where a partial alignment of the basic structural units and a decrease in the specific surface area observed [28].

exhibit very high surface areas, and carbon aerogels which have very low mass densities [27].

Porous activated carbon materials [see Fig. 5(a)] are generally synthesized through the reaction of carbon with O_2, H_2O and/or CO_2 in the temperature range $800 < T < 1200°C$ for pitch-based carbon fibers having diameters greater than 1 μm. One attraction of the activated carbon fibers over other porous carbon host materials is the relatively small pore size (< 2 nm) and the relatively narrow size distribution of these nano-pores. Current emphasis of basic research on porous carbons is on the study of the pore structures, and improved synthesis routes for the preparation of cheaper porous carbons with enhanced performance in terms of control of the pore size and the pore size distribution. Scientific systematic studies have used heat treatment [see Fig. 5(b)] and temperature-dependent measurements to gain insights into the structure and properties of these materials and the mechanisms controlling these properties [28,29]. Activated carbon fibers are used widely for adsorption and filtration applications for the purification of air and water (especially for the removal of SO_x and NO_x), as well as for electronic applications, such as capacitors for energy storage. Much of the advanced development research, process and product development, and the manufacture of activated carbon fibers is carried out in Japanese industry.

Carbon aerogels are a disordered form of sp^2-bonded carbon which are members of a family of low-density micro-cellular materials. Carbon aerogels have low mass densities, ρ_m, relatively large specific surface areas (600-800 m^2/g), and very high porosities. Carbon aerogels are synthesized by a super-cooling process [30]. Depending on the details of their synthesis, carbon aerogels exhibit two morphological types, polymeric and colloidal, each with its distinct structural characteristics. The aerogels of both types are built up by kinetic aggregation of molecular clusters, which typically have diameters of $\sim$12 nm. These very small ''primary nano-particles'' contain nanopores (< 2 nm), and the primary particles cluster together into a network of ''secondary nano-particles'', which give rise to mesopores (2–50 nm), as shown in Fig. 6. Mesopores of small size are also called micropores. The secondary nano-particles are, in turn, strung out in chains to create the porous matrix of the aerogel, with macropores (> 50 nm) located between chains. In contrast, the activated carbon fibers discussed above have a large density of nanopores, but few mesopores or macropores.

The primary nano-particles in carbon aerogels with diameters near 12 nm, are shown schematically in Fig. 6 [30,31]. Within each nano-particle, a glassy carbon–like nanostructure is observed, consisting of an intertwined network of narrow graphitic ribbons of width $\sim$2.5 nm. The morphology of the carbon aerogels is illustrated schematically in Fig. 6 for both a low density material ($\sim$0.1 g/cm^3) and a higher density material ($\sim$0.6 g/cm^3) [31]. This morphology leads to a relatively high specific surface area (600–800 m^2/g), with a wide distribution of pore diameters. For a given specific surface area, carbon aerogels tend to have larger size pores and a much larger

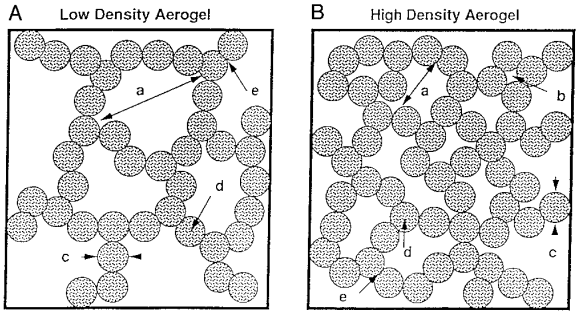

Fig. 6. Schematic diagram of the carbon aerogel microstructure. Each shaded circle represents a disordered carbon nano-particle. The microstructure is shown on the left for low ($\sim$0.1 g/cm^3) and on the right for high ($\sim$0.6 g/cm^3) bulk density forms of carbon aerogels. The microstructure shows (a) mesopores that span the distance between chains of interconnected nano-particles, (b) micropores sandwiched between nano-particles, (c) individual nano-particles ($\sim$12 nm diameter), (d) nanopores within the nano-particles, and (e) micropores between contiguous nano-particles [31].

distribution of pore sizes than the activated carbon fibers discussed above.

Because of their large surface areas and consequently high density of dangling bonds, porous carbons tend to have somewhat different electronic and transport properties from those of other disordered carbons. Activation of carbon aerogels leads to very lightweight materials with specific surface areas comparable to those in activated carbon fibers. Thus far there has been very little reported work on the structure and properties of *activated* carbon aerogels. Provided that the structural integrity of this material is adequate, we can expect activated carbon aerogels to have attractive properties for a host of energy-related applications.

A number of significant opportunities have been identified for carbon aerogel applications, including gas adsorption devices, separators for heavy metals and ions, purification of drinking water, and electronic capacitors. Current research activities focus on gaining a better understanding of the pore structure and its properties, initiating systematic studies of the structure and properties of activated carbon aerogels with surface areas up to perhaps 3000 m^2/g. The science and technology of carbon aerogels would attract much more attention than they now do, if cheaper synthesis routes could be found for the production of larger quantities of carbon aerogel material with enhanced and controlled properties.

The DOE laboratories have historically played a major role worldwide in the science and technology of carbon aerogels, and remains leaders in this field. Collaborations with researchers from academia have contributed significantly to the science base, while collaborations with industry have been fostered to promote practical applications. Some small start-up companies have also been spun-off. Carbon aerogels remain a promising area for DOE energy-related applications.

5. Fullerenes

Because of the relatively high energy cost of dangling bonds and edge sites on graphene sheets (which are single atomic layers of the crystalline graphite structure), small numbers of carbon atoms do not crystallize as planar structures. In contrast, small numbers n_C of carbon atoms rather form closed cage molecules (for $30 \leq n_C \leq 300$). The most common closed cage molecule by far is C_{60} which is in the form of a regular truncated icosahedron and has 12 pentagonal and 20 hexagonal faces, with every one of the 60 carbon atoms located at an equivalent site (see Fig. 7) [32,33]. These molecules are of sub-nanometer size (0.71 nm diameter) and every C_{60} molecule is identical to every other C_{60}, except for possible isotopic substitutions (^{13}C for ^{12}C with relative natural abundance $^{13}C/^{12}C \sim 0.011$). The discovery of the closed cage fullerene molecule in 1985 [32] opened up an exciting new research field which was extremely active during the early 1990s.

According to Euler's theorem for polygons, a polyhedron containing only hexagon and pentagon faces must have 12 pentagons, but can have an arbitrary number of hexagons. On this basis, one would expect C_{20} with only pentagon faces to be the smallest fullerene. Since the addition of one hexagon requires the addition of two carbon atoms, all fullerenes contain an even number of carbon atoms. Calculations show that the high local curvature of polyhedra containing adjacent pentagons yields a high free energy, so that stable fullerenes do not contain adjacent pentagonal faces, thus leading to the isolated pentagonal rule for stable fullerenes. The C_{60} molecule is the smallest fullerene molecule obeying the isolated pentagon rule, and there is only one way to arrange 60 carbon atoms into pentagons and hexagons in accordance with the isolated pentagon rule, as shown in Fig. 7(a). The high symmetry leads to high stability relative to the addition or subtraction of 2 carbon atoms, which is needed to form one hexagon. Thus C_{60} is by far the most abundant fullerene. The next most common fullerene is C_{70}, formed by the addition of 5 hexagons around the equator of C_{60} and normal to a 5-fold axis (as shown in Fig. 7). As for the case of C_{60}, there is a single unique way to arrange 70 carbon atoms into a fullerene satisfying the isolated pentagon rule. In

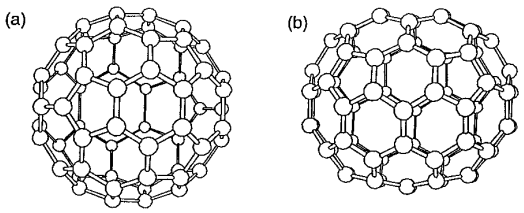

Fig. 7. (a) The icosahedral C_{60} molecule. (b) The C_{70} molecule as rugby ball–shaped (D_{5h} symmetry) [33].

general, fullerenes consisting of C_N carbon atoms can be formed with multiple geometric arrangements called isomers. For example, C_{78} can be formed with both C_{2v} symmetry and D_3 symmetry [33].

C_{60} molecules can be prepared by a variety of methods such as arc discharge, laser vaporization, and flame emission techniques. Almost all C_{60} and C_{70} is presently obtained from commercial sources using a method first developed by Krätschmer and Huffman [34] based on an alternating current arc discharge between graphite electrodes (20V, 60A) in approximately 200 torr of He. Separation and purification of C_{60} from C_{70} and the higher molecular weight fullerenes is typically accomplished using liquid chromatography (LC). Samples of C_{60} with $\geqslant 99\%$ purity are now commonly available. Liquid chromatography generally provides sensitivity for the separation of fullerenes according to their molecular weights and to some extent also according to their isomers.

Progress is still needed to increase the production efficiency, to improve the separation specificity and thereby increase the purity of each fullerene species, and above all to reduce costs in order to stimulate practical interest in potential applications for fullerenes. Since C_{60} and C_{70} fullerene production is now largely commercialized, many of the advances in the synthesis of these fullerenes can be expected to come from industry. However, the synthesis, separation, and purification of higher molecular weight fullerenes remain an active research area, together with study of the structure, stability and properties of these higher mass fullerenes and their isomers. Fundamental studies of the fullerene growth mechanism are still an important research area, including the development of novel synthesis routes which might enhance our understanding of the synthesis process, or could lead to more efficient and cheaper production processes. Synthetic chemists and biochemists continue to add functional groups to C_{60} to obtain molecules with especially desirable properties, such as water solubility.

For most scientific studies and practical applications, fullerenes are studied in the gas phase, in solution, or in microcrystalline powder samples, in films, or in single crystals. Pristine C_{60} films can be deposited onto a substrate such as clean Si(100) by vacuum sublimation of the C_{60} powder using vacuum science techniques. Ellipsometry is normally used to measure the thickness of the C_{60} films as they are deposited. High quality single crystals are primarily grown by vacuum sublimation. The growth of crystalline films is accomplished by lattice matching of the lattice constant of the fcc crystalline phase to the lattice constant of the substrate [33]. The surface science of fullerenes remains an active research field with regard to increasing our understanding of the fullerene-surface interaction and the charge transfer across the interface. Strong bonding occurs when the surface has an abundance of available bonds, such as metals or selected semiconductors like silicon with a high density of surface states or dangling bonds. Other surfaces with few dangling bonds, such as oxides, bind even less weakly to fullerenes than fullerenes bind to each other. The strong binding to Si and weak binding to SiO_2 can be utilized for high resolution lithography, taking advantage of the great uniformity of the molecules of the photo-resist [33].

The unique properties of C_{60} stem largely from the highly molecular character of crystalline C_{60} and the high symmetry of the C_{60} molecules. The molecular nature of crystalline fullerene solids is well established by studies of their electronic structure and phonon spectra. Of particular interest has been the study of the optical absorption edge that is dominated by forbidden, excitonic transitions that are phonon-assisted. The strong selection rules associated with these transitions give rise to outstanding properties of C_{60} for optical limiting applications, utilizing the higher absorption cross section for transitions originating from excited states relative to those originating from the ground state [33,35,36]. These optical studies remain an important area for current research, as discussed below.

Optical studies on crystalline C_{60} at room temperature have been difficult to carry out because optical excitations promote the bonding of adjacent C_{60} molecules, thereby lowering their symmetry and leading to a breakdown in the selection rules governing isolated C_{60} molecules or crystalline fcc C_{60} at low temperature. Since the dimerization (or polymerization) process is sensitive to light intensity, light frequency, temperature, pressure, the presence of oxygen and other experimental conditions [37–39], many of the early optical experiments have to be repeated under more controlled conditions to obtain definitive results. Systematic studies of the polymerization process itself are also being actively pursued by many groups worldwide, motivated by both basic science and by potential applications of a controlled

polymerization transformation process, as for example for use of C_{60} as photoresists with high spatial resolution.

Since the carbon atoms in the C_{60} molecules have all of their valence requirements satisfied, the crystalline solid derived from C_{60} is non-conducting, unless carriers are introduced by thermal or optical excitation or by appropriate chemical doping. In fact, the doping of C_{60} with the alkali metals M = K or Rb to the concentration M_3C_{60} leads to metallic conduction generally, and to superconducting behavior at low temperature with relatively high T_c values, the highest T_c value being ~40K for Cs_3C_{60} under pressure [40]. Because of the large volumes of the interstitial spaces between the fullerenes in the lattice, fullerenes can be doped with alkali metals, alkaline earths, and rare earth metal species, and this doping provides a method for studying the electronic structure of the conduction bands in crystalline fullerene arrays called fullerites. The ringing of the $A_g(1)$ radial breathing mode near 492 cm^{-1} in K_3C_{60} for more that 200 cycles after excitation by a short laser pulse (~20 fs duration) indicates that the C_{60} molecules can be coupled to each other electronically by doping and charge transfer, though the phonon modes remain molecular in nature [41,42]. Study of the transport mechanism in fullerene solids is an active research field, as is also study of the reason why metallic conduction only occurs for a narrow range in stoichiometry. Also attracting attention is the metallic and polymeric nature of the M_1C_{60} phase as well as the various crystalline phases of alkali metal doped fullerenes occurring at high pressures.

Fullerenes can also be doped by the insertion of guest species into the hollow core region to form endohedral fullerenes (see Fig. 8). The synthesis of endohedral fullerenes can be carried out either by arc discharge or laser vaporization methods, with the positive electrode material (in the case of the carbon arc) or the target material (in the case of laser vaporization) consisting of a composite of graphite and the endohedral dopant. Other synthesis and processing steps for preparing endohedral fullerenes are, in principle, similar to the corresponding steps for fullerenes. In practice, however, it has been difficult to prepare sufficient quantities of pure endohedral species to carry out systematic studies of their structure and properties. Therefore, emphasis has been given to developing more efficient synthesis routes in order to prepare greater quantities of purified and well characterized endohedral fullerenes. Once sufficient quantities of purified and well characterized samples are available, systematic studies of the structure and physical properties of endohedral fullerenes will be carried out, both in the molecular phase and in the crystalline phase.

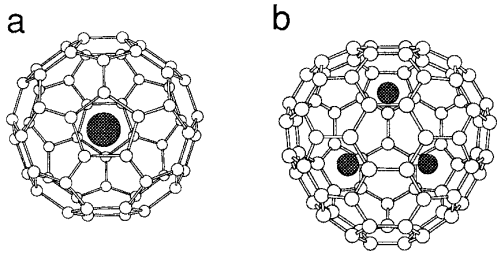

Fig. 8. Structural models for an endohedral fullerene with (a) a La^{3+} ion at the center of the C_{60} cage [43], and (b) three equivalent Sc ions, which rapidly reorient within the C_{82} cage [44].

For a number of endohedral species, the charge state of the endohedral dopant has been established, though less is known about the location of the dopant within the cage, as for example whether the dopant is at a central location, as shown in Fig. 8(a), or at a non-central location. Since it is possible to insert more than one ion endohedrally, as shown in Fig. 8(b), a large variety of endohedral fullerenes can be synthesized, as for example the addition of one, two or three Sc ions into C_{82}. The search for new endohedral species such as La, Y, Sc, especially those with promise for unique physical properties, continues to be an active research field. Because of the flexibility associated with the selection of endohedral species, it should be possible to prepare endohedral fullerenes with special magnetic and dielectric properties. Studies of the structure and properties of endohedral fullerenes in the crystalline phase under pressure should be another topic of future interest.

An energy-related applications area that has been widely discussed relates to the use of small concentrations of fullerenes to dope polymers and to control the properties of the resulting composite. In such fullerene–polymer composites photo-carrier excitation plays an important role in the charge transfer mechanism. In the case of C_{60}-polymer composites, photo-induced charge transfer creates C_{60} anions, leaving holes on the polymer chains, which are available for conduction [45]. Photo-induced charge transfer has also been discussed for

xerography applications, especially using C_{70}, because of its photo-sensitivity at longer wavelengths [46,47]. Another applications area that has been widely discussed is the use of fullerenes for drug delivery by suitable functionalization of the fullerenes [48,49]. C_{60} has also been used as a precursor for the growth of unusually smooth diamond films which are of interest for use in coating applications [50,51]. This smooth surface is directly related to the fine nanostructure of the diamond grains.

6. Carbon Nanotubes

Carbon nanotube research is probably the most active research field in carbon science at the present time. The experimental identification in 1991 of multi-wall carbon nanotubes [53] first attracted attention to the field. This observation stimulated a large number of theoretical works on the structure and properties of the simpler and more fundamental single-wall carbon nanotubes, one atomic layer in thickness in the radial direction (see Fig. 9). The experimental discovery of single-wall carbon nanotubes in 1993 [53,54] further stimulated work in the field, though, at first, only small quantities of single-wall nanotubes were available experimentally for systematic studies. These single-wall nanotubes were generally found along with very much larger concentrations of carbon nanoparticles and other carbon-based materials, and the single-wall constituents contained a broad distribution of diameters and geometries, as explained below. For these reasons most of the experimental studies continued to be done on multi-wall nanotubes. The recent discovery in 1996 of a much more efficient synthesis route, involving laser vaporization of graphite [55], to prepare arrays of ordered single-wall nanotubes, offers major new opportunities for quantitative experimental studies of carbon nanotubes and is having a large impact on the field.

The fundamental carbon nanotube is a single-wall structure which has three basic geometries as shown in Fig. 9. Carbon nanotubes are capped at either end by half of a fullerene, so that the smallest diameter nanotube corresponds to the smallest diameter fullerene (C_{60}) which has a diameter of 7.1 Å. The structure of the nanotube can be understood by referring to Fig. 10, which demonstrates the rolling of a segment of a single graphite layer (called a graphene sheet) into a cylinder. In this figure we see that points O and A are crystallographically equivalent on a graphene sheet. The points O and A can be

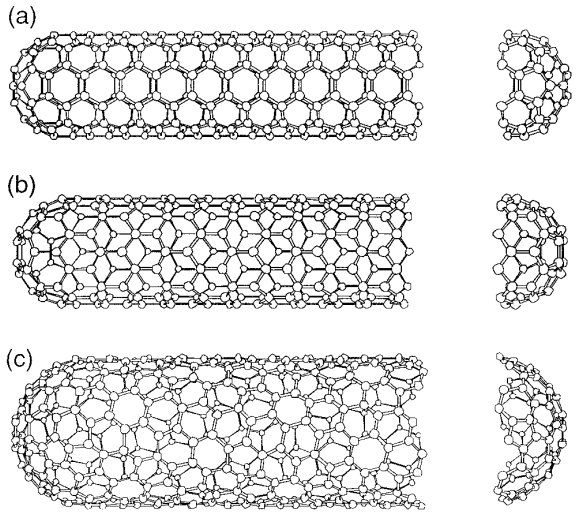

Fig. 9. Schematic models for a single-wall carbon nanotubes with the nanotube axis normal to: (a) the $\theta = 30^\circ$ direction (an ''armchair'' (n, n) nanotube), (b) the $0 < \theta = 30^\circ$ direction (a ''zigzag'' (n, 0°) nanotube), and (c) a general direction, such as $\overrightarrow{OA}$ (see Fig. 10), with $0 < \theta < 30^\circ$ (a ''chiral'' (n, m) nanotube). The actual nanotubes shown here correspond to (n, m) values of: (a) (5, 5), (b) (9, 0), and (c) (10, 5) [56].

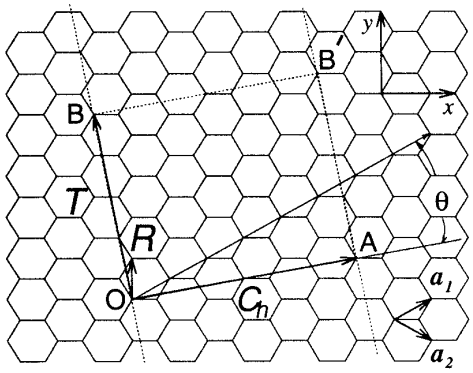

Fig. 10. The chiral vector $\overrightarrow{OA}$ or $\vec{C}_h = n\hat{a}_1 + m\hat{a}_2$ is defined on the honeycomb lattice of carbon atoms by unit vectors $\hat{a}_1$ and $\hat{a}_2$ and the chiral angle θ with respect to the zigzag axis. Along the zigzag axis $\theta = 0^\circ$. Also shown is the lattice vector OB of the 1D nanotube unit cell. The rotation angle ψ and the translation τ constitute the basic symmetry operation $R = (\psi|\tau)$ for the carbon nanotube. The diagram is constructed for $(n, m) = (4, 2)$. The area defined by the rectangle $(OAB'B)$ is the area of the 1D unit cell of the nanotube. The nearest neighbor carbon–carbon distance is taken as 1.42 Å, as in graphite.

connected by a chiral vector $\vec{C}_h = n\hat{a}_1 + m\hat{a}_2$, where $\hat{a}_1$ and $\hat{a}_2$ are unit vectors for the honeycomb lattice of the graphene sheet. Lines OB and AB' are normals to $\vec{C}_h$ at points O and A, and if we now superimpose OB onto AB', then we obtain a cylinder of carbon atoms which constitutes a carbon nanotube when properly capped at both ends with half of a fullerene. A single-wall carbon nanotube is thus uniquely determined by the integers (n, m) which specify the chiral vector $\vec{C}_h$, or equivalently by its diameter $d_t = |\vec{C}_h|/\pi$ and the chiral angle θ which $\vec{C}_h$ makes with the zigzag direction $(\theta = 0)$, as shown in Fig. 10. The unit cell of the 1D carbon nanotube is a rectangle formed by the vectors $\vec{C}_h$ and $\vec{T}$ shown in Fig. 10 where $\vec{T}$ is the smallest lattice vector from O in the direction normal to $\vec{C}_h$. Since the basis vectors $\vec{C}_h$ and $\vec{T}$ of the 1D unit cell are large compared with those of the unit cell for the graphene sheet, the reciprocal space unit cell (Brillouin zone) is small compared to that for the graphene sheet.

Single-wall carbon nanotubes are interesting examples of a one-dimensional periodic structure along the axis of the nanotube. Confinement in the radial direction is provided by the monolayer thickness of the nanotubes. In the circumferential direction, periodic boundary conditions apply to the enlarged unit cell that is formed in real space and the subsequent zone folding in reciprocal space of the dispersion relations for a graphene sheet into the Brillouin zone for the 1D nanotube. Zone-folding arguments have been used to obtain 1D dispersion relations for electrons [57–59] and phonons [60,61] in single-wall carbon nanotubes.

Calculation of these dispersion relations shows remarkable electronic properties, namely that for small diameter graphene nanotubes, about $\frac{1}{3}$ of the nanotubes are metallic and $\frac{2}{3}$ are semiconducting, depending on their fiber diameter d_t and chiral angle θ. Metallic conduction in a carbon nanotube is achieved when $2n + m = 3q$, where n and m are integers specifying the nanotube diameter and chiral angle, and q is an integer. The calculations show that all armchair (n, n) nanotubes are metallic, but only $\frac{1}{3}$ of the possible zigzag nanotubes are metallic [57–59], and likewise for the chiral nanotubes. Scanning tunneling microscopy/spectroscopy (STM/STS) studies [62] confirm that some nanotubes are metallic and some are semiconducting, and show that the bandgap for the semiconducting nanotubes is proportional to the reciprocal of the nanotube diameter, independent of nanotube chirality, in agreement with theoretical predictions [33].

The availability of ordered single-wall nanotube arrays (on a 2D triangular lattice) in which many of the nanotubes have the armchair (n, n) structure with $n \sim 10$ (corresponding to an average reported diameter of 1.38 ± 0.02 nm) [55] has greatly increased the research activity on single-wall nanotubes and has stimulated a wide variety of property measurements, especially studies emphasizing the one-dimensional quantum aspects of carbon nanotubes [63,64]. Measurement of the temperature dependence of the resistivity of ropes (arrays) of single-wall armchair carbon nanotubes [55] confirm the theoretical calculations that armchair nanotubes are metallic.

Transport measurements on an individual multi-wall nanotube have shown a variety of properties, with some differences from one multi-wall nanotube to another [65–67], as well as weak localization and universal conductance phenomena in the low temperature regime [67]. Research opportunities remain for systematic studies of these very interesting transport phenomena in the small diameter range where 1D phenomena are expected. There is particular interest in studying the dependence of these phenomena on nanotube diameter and chirality. Theoretical models should also be developed to explain weak localization and universal conductance phenomena for multi-wall carbon nanotubes.

More recently, transport measurements have been made on an individual single-wall carbon nanotube of about 1 nm diameter [64] and on an array (rope) of single-wall carbon nanotubes [63]. These studies focus on the quantum dot aspect of single-wall carbon nanotubes. Although carbon nanotubes are very long in comparison to their diameter, they are nevertheless finite in length. Because of their finite length, the nanotubes have discrete energy states and exhibit Coulomb blockade phenomena for the addition of a single electron to the nanotube. Charging energies of $E_c = e^2/2C = 2.6$ meV and energy separations of 0.6 meV between the discrete states near the Fermi level have been reported for a nanotube 3 μm in length [64]. Since armchair (n, n) carbon nanotubes are metallic and do not exhibit a Peierls gap, and because of their large length to diameter ratio, electrical contacts can be made to these nanometer size structures by modern lithographic techniques. Single-wall carbon nanotubes

thus provide a unique system for studying single molecule transistor effects [68,69]. Systematic studies of the Coulomb blockade phenomena as a function of nanotube diameter in armchair nanotubes and in other metallic nanotubes are of great current interest [69].

The junction between a semiconductor and a metallic nanotube offers another means for controlling the current flow through perturbations introduced in the junction region. Progress that has been made thus far in understanding the structure and properties of the junction region between two dissimilar carbon nanotubes [68,70–72] is encouraging and should stimulate further experimental and theoretical work, as well as discussions for applications.

Using the same zone-folding method for a 2D graphene sheet as was used to obtain the 1D electronic dispersion relations, the 1D phonon dispersion relations for carbon nanotubes have been calculated [61,73]. The zone folding method yields a large number of phonon modes, but only a few of the $q = 0$ vibrational modes are Raman or infrared active, the others being optically silent for a first-order process. Since the number of Raman-active and infrared-active modes for a given symmetry category is independent of nanotube diameter, the dependence of a particular vibrational mode on nanotube diameter can be investigated. Many of the mode frequencies and their Raman cross sections are found to be highly sensitive to the nanotube diameter, while others are not. Figure 11 shows the Raman spectrum for a sample that contains predominantly armchair (9,9) and (10,10) carbon nanotubes [74]. Prominent in this spectrum are a number of modes near 1580 cm^{-1} which exhibit a weak dependence on nanotube diameter and a strong mode at $\sim$186 cm^{-1} (an A_{1g} radial breathing mode) which is strongly dependent on the diameter.

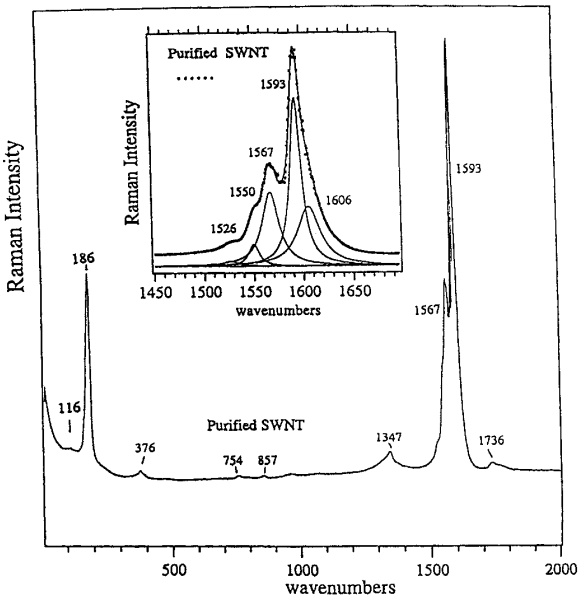

Fig. 11. Experimental Raman spectrum from a sample consisting primarily of single-wall armchair [74] nanotubes with diameters near that of the (10,10) nanotube.

Quantum effects are observed in the Raman spectrum through the resonant Raman intensity enhancement that occurs when the laser excitation frequency corresponds to a transition between the sharp features in the one-dimensional electronic states of the carbon nanotube. Since these sharp features in the density of states are strongly dependent on the nanotube diameter, a change in the laser frequency brings into resonance a different carbon nanotube, corresponding to a different diameter and characteristic vibrational frequency for the A_{1g} breathing mode. The observation of these quantum effects lend strong credibility to the 1D aspects of the electronic and phonon structure of single-wall carbon nanotubes.

In addition to research on the quantum phenomena, we can expect extensive research to continue on the growth mechanisms for both the single-wall and multi-wall nanotubes. Whereas multi-wall nanotubes require no catalyst for their growth, catalyst particles are necessary for the growth of the single-wall nanotubes. The detailed mechanisms for the growth of these nanotubes are not yet understood. We can also expect that a large effort will be made to refine present synthesis routes and to develop new routes that provide more controlled growth of nanotubes with the same diameter d_t and chiral angle θ. Right now there are methods available for the preferred synthesis of (10,10) armchair nanotubes [55]. Further synthesis work will focus on the growth of specific zigzag and chiral nanotubes, as well as on the growth of arrays of armchair nanotubes with controlled diameters.

Another area where there are exciting research opportunities involves the mechanical properties of carbon nanotubes. Research efforts thus far emphasize their very high modulus and strength [75], yet single-wall nanotubes show remarkable flexibility, can be bent around small circles or elongated by large amounts without breaking, and exhibit good mechanical properties on both extension and compression

[76]. These excellent mechanical properties can be used for applications directly, or in composites of carbon nanotubes with other materials or in conjunction with other properties that are utilized for applications. For example, a small concentration of carbon nanotubes is expected to significantly increase the strength of a polymer-based composite, without greatly increasing its viscosity, so that extrusion can be utilized in the forming of desired shapes.

Many research opportunities exist for the development of sensitive characterization techniques for objects 1 nm in size and for the controlled manipulation of such objects. Advances made in the characterization and manipulation of carbon nanotubes should have a substantial impact on the science and technology of nanometer structures more generally. The exceptionally high modulus and strength of carbon nanotubes makes them attractive for use in the manipulation of other small objects.

The caps of carbon nanotubes are more reactive than the cylindrical sections [77] and have been shown to be efficient electron emitters [78–80]. Applications of nanotubes for displays and for electron probe tips have thus been proposed. The ability of carbon nanotubes to retain relatively high gas pressures within their hollow cores indicate another area for applications. Carbon nanotubes have also been proposed as a flexible starting point for the synthesis of new nano-scale and nanostructured carbides [81,82]

It is expected that carbon nanotube research will be very active for several years into the future as quantum effects and other unique features are explored in the electronic structure, lattice modes, Raman and infrared spectra, transport properties, and mechanical properties of single-wall carbon nanotubes. The remarkable properties of carbon nanotubes also suggest opportunities for future applications.

7. Concluding Remarks

The last few years have seen the emergence of a variety of nanostructured π-bonded carbon materials, most notably the closed cage fullerene molecules, and the single-wall carbon nanotubes. The high present level of research activity on these carbon nanomaterials is likely to lead to important scientific advances in the nanostructures field generally, and hopefully useful applications will soon follow. Continued progress with the science and applications of more mature nanostructured carbon-based materials, such as carbon nanofibers and nanoporous carbons, is also expected. Because of the complexity of the carbon phase diagram and the unique locations of carbon in the periodic table, it is likely that other interesting nanostructured forms of carbon will be discovered in the near future, and that these new carbon materials will also lead to interesting science and perhaps also to useful applications. The authors gratefully acknowledge support from DOE grant #DE-FG02-94ER30231 for this work.

References

1. M.S. Dresselhaus, G. Dresselhaus, K. Sugihara, I.L. Spain, and H.A. Goldberg, *Graphite Fibers and Filaments* (Springer-Verlag, Berlin, 1988), Vol. 5 of *Springer Series in Materials Science*.
2. M. Endo, *CHEMTECH*, **18**, 568 (1988).
3. M. Endo and H.W. Kroto, *J. Phys. Chem.*, **96**, 6941 (1992).
4. M. Endo, K. Takeuchi, S. Igarashi, K. Kobori, M. Shiraishi, and H.W. Kroto, *J. Phys. Chem. Solids*, **54**, 1841 (1993).
5. M. Endo, K. Takeuchi, K. Kobori, K. Takahashi, H. Kroto, and A. Sarkar, *Carbon*, **33**, 873 (1995).
6. N.M. Rodriquez, *J. Mater. Res.*, **8**, 3233–3250 (1993).
7. M.S. Dresselhaus, G. Dresselhaus, P.C. Eklund, R. Saito, and M. Endo. In *Carbon Nanotubes: Preparation and Properties*, edited by T. Ebbesen, pages 1–33, CRC Press, Inc., Boca Raton, Florida, USA, 1997. Chapter I.
8. C. Niu, E.K. Sichel, R. Hoch, D. Moy, and H. Tennent, *Appl. Phys. Lett.*, **70**, 1480–82 (1997).
9. B. Miller, *Plastics World* (September 1996).
10. Minqi Liu and J.M. Cowley, *Carbon*, **32**, 393 (1994).
11. M. Liu and J.M. Cowley, *Ultramicroscopy*, **53**, 333 (1994).
12. Y. Saito, T. Yoshikawa, M. Okuda, M. Ohkohchi, Y. Ando, A. Kasuya, and Y. Nishina, *Chem. Phys. Lett.*, **209**, 72 (1994).
13. Y. Saito, *Carbon*, **33**, 979 (1995).
14. D. Ugarte, *Nature* (London) **359**, 707 (1992). see also: ibid H.W. Kroto, p. 670.
15. D. Ugarte, *Chem. Phys. Lett.*, **207**, 473 (1993).
16. D. Ugarte, *Carbon*, **33**, 989 (1995).
17. H. Kroto, *Nature* (London) **359**, 670 (1992).
18. D. Ugarte, *Europhys. Lett.*, **22**, 45 (1993).
19. J.S. Speck, *J. Appl. Phys.*, **67**, 495 (1990).
20. A. Maiti, J. Bravbec, and J. Bernholc, *Phys. Rev. Lett.*, **70**, 3023 (1993).
21. D. Tománek, W. Zhong, and E. Krastev, *Phys. Rev. B*, **48**, 15461 (1993).
22. K. Yamada, H. Kunishige, and A.B. Sowaoka, *Naturwissenschaften*, **78**, 450 (1991).
23. N. Hatta and K. Murata, *Chem. Phys. Lett.*, **217**, 398 (1994).
24. L.S. Weathers and W.A. Basset, *Phys. Chem. Minerals*, **15**, 105 (1987).
25. V.L. Kuznetsov, A.L. Chuvilin, Y.V. Butenko, I.Y. Mal'kov, and V.M. Titov, *Chem. Phys. Lett.*, **222**, 343 (1994).

26. F. Banhart and P.M. Ajayan, *Nature* (London) **382**, 433–35 (1996).
27. R. Pekala, C.T. Alviso, F.M. Kong, and S.S. Hulsey, *J. Non-Cryst. Solids*, **145**, 90–8 (1992).
28. M.S. Dresselhaus, A.W.P. Fung, A.M. Rao, S.L. di Vittorio, K. Kuriyama, G. Dresselhaus, and M. Endo, *Carbon*, **30**, 1065–73 (1992).
29. A.W.P. Fung, K. Kuriyama, A.M. Rao, M.S. Dresselhaus, G. Dresselhaus, and M. Endo, *J. Mat. Sci.*, **8**, 489–500 (1993).
30. R.W. Pekala and C.T. Alviso. In *Novel Forms of Carbon*, edited by C.L. Renschler, J.J. Pouch and D.M. Cox, pages 3–14, Materials Research Society, Pittsburgh, PA, 1992. Vol 270.
31. A.W.P. Fung, Z.H. Wang, K. Lu, M.S. Dresselhaus, and R.W. Pekala, *J. Mat. Res.*, **8**, 1875 (1993).
32. H.W. Kroto, J.R. Heath, S.C. O'Brien, R.F. Curl, and R.E. Smalley, *Nature* (London) **318**, 162–63 (1985).
33. M.S. Dresselhaus, G. Dresselhaus, and P.C. Eklund, *Science of Fullerenes and Carbon Nanotubes* (Academic Press, New York, NY, 1996).
34. W. Krätschmer, L.D. Lamb, K. Fostiropoulos, and D.R. Huffman, *Nature* (London) **347**, 354–58 (1990).
35. L.W. Tutt and A. Kost, *Nature* (London) **356**, 225 (1992).
36. J.E. Wray, K.C. Liu, C.H. Chen, W.R. Garrett, M.G. Payne, R. Goedert, and D. Templeton, *Appl. Phys. Lett.*, **64**, 2785 (1994).
37. A.M. Rao, P. Zhou, K.-A. Wang, G.T. Hager, J.M. Holden, Ying Wang, W.T. Lee, Xiang-Xin Bi, P.C. Eklund, D.S. Cornett, M.A. Duncan, and I.J. Amster, *Science*, **259**, 955–57 (1993).
38. Y. Wang, J.M. Holden, Z.H. Dong, X.X. Bi, and P.C. Eklund, *Chem. Phys. Lett.*, **211**, 341 (1993).
39. U.D. Venkateswaran, M.G. Schall, Y. Wang, P. Zhou, and P.C. Eklund, *Solid State Commun.*, **96**, 951 (1995).
40. T.T.M. Palstra, O. Zhou, Y. Iwasa, P. Sulewski, R. Fleming, and B. Zegarski, *Solid State Commun.*, **93**, 327 (1995).
41. Siegfried Fleischer. *Ultrafast dynamics studies on fullerene thin films*. PhD thesis, Massachusetts Institute of Technology, February 1997. Department of Electrical Engineering and Computer Science.
42. S.B. Fleischer, B. Pevzner, D.J. Dougherty, H.J. Zeiger, G. Dresselhaus, M.S. Dresselhaus, E.P. Ippen, and A.F. Hebard, (unpublished).
43. S. Saito, S. Sawada, and N. Hamada, *Phys. Rev. B*, **45**, 13845 (1992).
44. D.M. Poirier, M. Knupfer, J.H. Weaver, W. Andreoni, K. Laasonen, M. Parrinello, D.S. Bethune, K. Kikuchi, and Y. Achiba, *Phys. Rev. B*, **49**, 17403 (1994).
45. N.S. Sariciftci, L. Smilowitz, C. Zhang, V.I. Srdanov, A.J. Heeger, and F. Wudl, *Proc. SPIE - Int. Soc. Opt. Eng.*, **1852**, 297–307 (1993).
46. A. Hirao, H. Nishizawa, H. Miyamoto, M. Sugiuchi, and M. Hosoya. In *Proceedings of the International Society for Optical Engineering (SPIE)*, edited by Z. H. Kafafi, pages 71–80, SPIE Optical Engineering Press, Bellingham, WA, 1995. vol 2526, San Diego, CA, July 13, 1995.
47. M. Hosoya, K. Ichimura, Z.H. Wang, G. Dresselhaus, M.S. Dresselhaus, and P.C. Eklund, *Phys. Rev. B*, **49**, 4981 (1994).
48. C. Toniolo, A. Bianco, M. Maggini, G. Scorrano, M. Prato, M. Marastoni, R. Tomatis, S. Spisani, G. Palu, and E.D. Blair, *J. Med. Chem.*, **37**, 4558–62 (1994).
49. T. Tsuchiya, Y.N. Yamakoshi, and N. Miyata, *Biochem. Biophys. Res. Commun.*, **206**, 885–94 (1995).
50. D.M. Gruen, Shengzhong Liu, A.R. Krauss, and Xianzheng Pan, *J. Appl. Phys.*, **75**, 1758 (1994).
51. D.M. Gruen, A.R. Krauss, C.D. Zuiker, R. Csencsits, L.J. Terminello, J.A. Carlisle, I. Jimenez, G.J. Sutherland, D.K. Shuh, W. Tong, and F.J. Himpsel, *Appl. Phys. Lett.*, **68**, 1640–42 (1996).
52. S. Iijima, *Nature* (London) **354**, 56 (1991).
53. S. Iijima and T. Ichihashi, *Nature* (London) **363**, 603 (1993).
54. D.S. Bethune, C.H. Kiang, M.S. de Vries, G. Gorman, R. Savoy, J. Vazquez, and R. Beyers, *Nature* (London) **363**, 605 (1993).
55. A. Thess, R. Lee, P. Nikolaev, H. Dai, P. Petit, J. Robert, C. Xu, Y.H. Lee, S.G. Kim, A.G. Rinzler, D.T. Colbert, G.E. Scuseria, D. Tománek, J.E. Fischer, and R.E. Smalley, *Science*, **273**, 483 (1996).
56. M.S. Dresselhaus, G. Dresselhaus, and R. Saito, *Carbon*, **33**, 883–891 (1995).
57. R. Saito, M. Fujita, G. Dresselhaus, and M.S. Dresselhaus, *Appl. Phys. Lett.*, **60**, 2204–06 (1992).
58. J.W. Mintmire, B.I. Dunlap, and C.T. White, *Phys. Rev. Lett.*, **68**, 631–34 (1992).
59. T. Hamada, M. Furuyama, T. Tomioka, and M. Endo, *J. Mater. Res.*, **7**, 1178–88 (1992). ibid., 2612–20.
60. Latha Venkataraman. *Calculation of the Phonon Modes in Carbon Nanotubes*, June 1993. Bachelor of Science thesis, Department of Physics, MIT.
61. R.A. Jishi, L. Venkataraman, M.S. Dresselhaus, and G. Dresselhaus, *Chem. Phys. Lett.*, **209**, 77–82 (1993).
62. C.H. Olk and J.P. Heremans, *J. Mater. Res.*, **9**, 259 (1994).
63. M. Bockrath, D.H. Cobden, P.L. McEuen, N.G. Chopra, A. Zettl, A. Thess, and R.E. Smalley, *Science*, **275**, 1922 (1997).
64. S.J. Tans, M.H. Devoret, H. Dal, A. Thess, R.E. Smalley, L.J. Geerligs, and C. Dekker, *Nature* (London) **386**, 474 (1997).
65. H. Dai, E.W. Wong, and C.M. Lieber, *Science*, **272**, 523–26 (1994).
66. T.W. Ebbesen, H.J. Lezec, H. Hiura, J.W. Bennett, H.F. Ghaemi, and T. Thio, *Nature* (London) **382**, 54–6 (1996).
67. L. Langer, V. Bayot, E. Grivei, J.P. Issi, J.P. Heremans, C.H. Olk, L. Stockman, C. Van Haesendonck, and Y. Bruynseraede, *Phys. Rev. Lett.*, **76**, 479–82 (1996).
68. M.S. Dresselhaus, *Physics World*, pages 18–19 (May 1996). Review.
69. L. Kouwenhoven, *Science*, **275**, 1896 (1997).
70. R. Saito, G. Dresselhaus, and M.S. Dresselhaus, *Phys. Rev. B*, **53**, 2044 (1996).
71. L. Chico, V.H. Crespi, L.X. Benedict, S.G. Louie, and M.L. Cohen, *Phys. Rev. Lett.*, **76**, 971 (1996).
72. Ph. Lambin, A. Fonseca, J.P. Vigneron, J.B. Nagy, and A.A. Lucas, *Chem. Phys. Lett.*, **245**, 85 (1995).
73. R.A. Jishi, D. Inomata, K. Nakao, M.S. Dresselhaus, and G. Dresselhaus, *J. Phys. Soc. Jpn.*, **63**, 2252–60 (1994).
74. A.M. Rao, E. Richter, S. Bandow, B. Chase, P.C. Eklund, K.W. Williams, M. Menon, K.R. Subbaswamy, A. Thess, R.E. Smalley, G. Dresselhaus, and M.S. Dresselhaus, *Science*, **275**, 187–91 (1997).
75. M.M.J. Treacy, T.W. Ebbesen, and J.M. Gibson, *Nature* (London) **381**, 678 (1996).

76. B.I. Yakobson and R.E. Smalley, *American Scientist*, **85**, in press (1997).
77. D.L. Carroll, P. Redlich, P.M. Ajayan, J.C. Charlier, X. Blase, A. De Vita, and R. Car, *Phys. Rev. Lett*., **78**, 2811 (1997).
78. W.A. de Heer, A. Châtelain, and D. Ugarte, *Science*, **270**, 1179 (1995). see also ibid page 1119.
79. A.G. Rinzler, J.H. Hafner, P. Nikolaev, L. Lou, S.G. Kim, D. Tománek, P. Nordlander, D.T. Colbert, and R.E. Smalley, *Science*, **269**, 1550 (1995).
80. P.G. Collins and A. Zettl, *Appl. Phys. Lett*., **69**, 1969 (1996).
81. H. Dai, E.W. Wong, Y.Z. Lu, S. Fan, and C.M. Lieber, *Nature* (London), 769 (1995).
82. E.W. Wong, B.W. Maynor, L.D. Burns, and C.M. Lieber, *Chem. Mater*., **8**, 2041 (1996).